Inorg. Chem. **2005**, *44*, 7494–7502

Oxygen Atom Transfer Reactivity from a Dioxo-Mo(VI) Complex to Tertiary Phosphines: Synthesis, Characterization, and Structure of Phosphoryl Intermediate Complexes

Victor N. Nemykin[§] and Partha Basu*

Department of Chemistry and Biochemistry, Duquesne University, Pittsburgh, Pennsylvania 15282

Received May 23, 2005

The oxygen atom transfer (OAT) reactivity of Tp^*MoO_2Cl with PMe_3, PEt_3, and $PPhMe_2$ (where Tp^* = hydrotris-(3,5-dimethylpyrazol-1-yl)borate) has been investigated. The OAT reactions proceed through a diamagnetic Mo(IV) phosphoryl intermediate complex of general formula $Tp^*MoOCl(OPR_3)$ (OPR_3 = $OPMe_3$, $OPEt_3$, $OPPhMe_2$), which have been isolated and characterized by ^1H and ^{31}P NMR, UV–visible, and infrared spectroscopies and electrospray ionization mass spectrometry. Solid-state crystal structures of $Tp^*MoOCl(OPMe_3)$ and $Tp^*MoOCl(OPPhMe_2)$ are also reported, the oxygen-to-phosphorus distances agree with a double-bond formulation and a single bond between the metal and the phosphoryl oxygen atom. The stability of the phosphoryl intermediate complexes depends on the steric properties of the coordinated phosphine-oxides. These intermediate complexes have been converted to solvent-coordinated species, Tp*MoOCl(solv) (solv = acetonitrile or dmf), and the coordinated solvents exchange with the bulk solvent.

Introduction

Mononuclear molybdopterin enzymes catalyze the net transfer of an oxygen atom between substrate and water, as shown in eq 1. The molybdenum center in enzymes of the sulfite oxidase (SO) family shuttles between a dioxo-molybdenum(VI)

$$X + H_2O \leftrightarrow XO + 2H^+ + 2e^- \qquad (1)$$

($[Mo^{VI}O_2]^{2+}$) and a monooxo-molybdenum(IV) ($[Mo^{IV}O]^{2+}$) state during the course of catalysis. Studies from several laboratories have demonstrated that a variety of discrete oxo-molybdenum complexes can carry out atom transfer chemistry when reacted with oxygen atom abstractors, producing oxidized species such as tertiary phosphines oxides, sulfoxides, *N*-oxides, tertiary arsine-oxide, or sulfate.[1−7] Although tertiary phosphines are not physiological substrates, they are the most commonly used substrates for studying oxygen atom transfer (OAT) reactions in model compounds, and have been observed to exhibit OAT reactivity with DMSO reductases.[8] Analogue chemistry has played important roles in describing the overall reaction. To this end, compounds stabilized by enedithiolate or hydrotris(pyrazolyl)borate ligands have contributed significantly.[1]

About 10 years ago, a theoretical study[9] proposed that dioxo-molybdenum(VI) centers react with tertiary phosphines generating a phosphines oxide-coordinated intermediate complex. Subsequently, we described the synthesis and characterization of phosphines oxide-coordinated compound by reacting a dioxo-Mo(VI) complex with tertiary

* To whom correspondence should be addressed. E-mail: basu@duq.edu.
§ Current address: Department of Chemistry and Biochemistry, University of Minnesota Duluth, Duluth, MN 55812.

(1) Enemark, J. H.; Cooney, J. J. A.; Wang, J.-J.; Holm, R. H. *Chem. Rev.* **2004**, *104*, 1175−1200.
(2) Holm, R. H. *Coord. Chem. Rev.* **1990**, *100*, 183−221.
(3) Pilato, R. S.; Stiefel, E. I. In *Bioinorganic Catalysis*, 2nd ed.; Reedijk, J., Bouwman, E., Eds.; Marcel Dekker: New York, 1999; pp 81−152.
(4) McMaster, J.; Tunney, J. M.; Garner, C. D. *Prog. Inorg. Chem.* **2003**, *52*, 539−583.
(5) Young, C. G. In *Biomimetic Oxidations Catalyzed by Transition Metal Complexes*; Meunier, B., Ed.; Imperial College Press: London, 2000; p 415−459.
(6) Donahue, J. P.; Goldsmith, C. R.; Nadiminti, U.; Holm, R. H. *J. Am. Chem. Soc.* **1998**, *120*, 12869−12881. Lorber, C.; Plutino, M. R.; Elding, L. I.; Nordlander, E. *J. Chem. Soc., Dalton Trans.* **1997**, 3997−4004. Das, S. K.; Chaudhury, P. K.; Biswas, D.; Sarkar, S. *J. Am. Chem. Soc.* **1994**, *116*, 9061−9070. Wang, J.-J.; Kryatova, O. P.; Rybak-Akimova, E. V.; Holm, R. H. *Inorg. Chem.* **2004**, *43*, 8092−8101. Chaudhury, P. K.; Nagarajan, K.; Dubey, P.; Sarkar, S. *J. Inorg. Biochem.* **2004**, *98*, 1667−1677.
(7) Jiang, J.; Holm, R. H. *Inorg. Chem.* **2005**, *44*, 1068−1072.
(8) Schultz, B. E.; Hille, R.; Holm, R. H. *J. Am. Chem. Soc.* **1995**, *117*, 827−828.
(9) Pietsch, M. A.; Hall, M. B. *Inorg. Chem.* **1996**, *35*, 1273−1278.

10.1021/ic0508324 CCC: $30.25
Published on Web 09/21/2005

Scheme 1

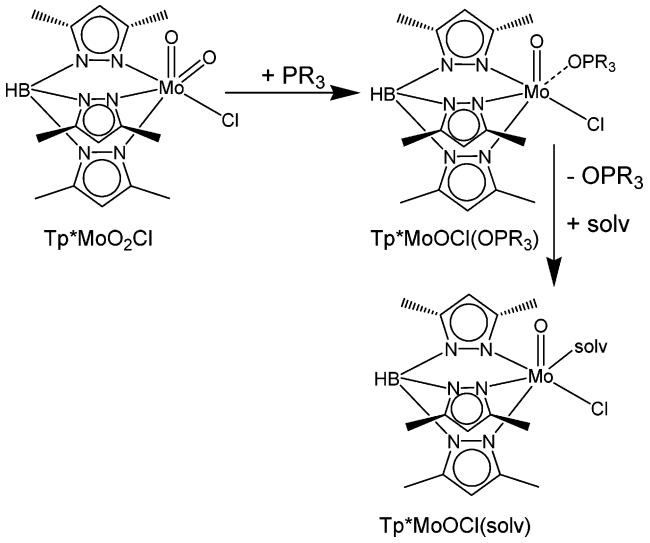

phosphines, which underscores the multistep nature of the OAT reaction. Currently, OAT reactions are described in terms of at least two transition states,[10,11] where one transition state relates to the formation of the intermediate complex and the second transition state describes the product release.

The OAT reactivity from dioxo-Mo(VI) centers coordinated by the hydrotris(pyrazolyl) borate ligand is schematically presented in Scheme 1. It includes the formation of the intermediate molecule of general formula of Tp*MoOX-(OPR_3) and the solvated complex of general formula of Tp*MoOX(solv). The pyridine-coordinated complexes of general formula Tp*MoOX(py) (X= Cl, SPh) have been reported previously.[12] More recently, we have reported the synthesis and characterization of phosphoryl species Tp^{iPr}MoOX(OPR_3) (OPR_3 = $OPEt_3$, $OPPh_2Et$; X = chloride, phenolates, and thiolates; Tp^{iPr} = hydrotris(3-isopropyl-pyrazol-1-yl)borate).[13] In this system, a bulkier Tp^{iPr} ligand has been used in stabilizing the phosphoryl intermediate complexes. The presence of the bulky isopropyl group and the absence of any substituents at the 3-position of the pyrazole rings allow the ligand to adopt a larger bite angle, and as a result, higher stability of the phosphoryl intermediates have been achieved.

In the case of the simpler Tp* system, it has been reported that the rate of the overall OAT reactions of Tp*MoO_2X with PPh_3 depends on the equatorial ligand such that X = Cl ≫ SR > OR, suggesting that the reaction proceeds more efficiently with Tp*MoO_2Cl.[12] This small molecule rapidly reacts with PPh_3, and the intermediate compound could be detected by mass spectrometry.[14] Using a smaller phosphine (PMe_3), we have recently communicated the synthesis of Tp*MoOCl($OPMe_3$) and the thermodynamic analysis of the reaction of Tp*MoO_2Cl with PMe_3.[15] In this paper, we describe complete details of isolation, characterization, electronic, and steric properties of a new series of complexes of general formula Tp*MoOCl(OPR_3) (PMe_3, PEt_3 and $PPhMe_2$) and their behavior in solution. The isolation and complete characterization of the solvent-coordinated species, Tp*MoOCl(solv) (solv= dmf, MeCN), their spectra, and their electronic structures are also discussed. The electronic spectra have been analyzed with the aid of density functional theory. The current molecules represent one of the simplest molecular system to exhibit the OAT reactivity.

Experimental Section

All syntheses were conducted using standard Schlenk techniques or inside an inert-atmosphere drybox under dry Ar or N_2 atmospheres. Solvents were purchased from commercial sources such as the Aldrich Chemical Co. and the Acros Chemical Co. and purified as before.[16] All mass spectra were collected in a Micromass ZMD quadrupole spectrometer equipped with ESI source in a positive-ion mode, using acetonitrile (AN) as the mobile phase. The nebulizer tip was set at 3.5 kV and 80 °C, and dry nitrogen was used as the bath gas. UV−visible spectra were recorded on a modified temperature-controlled Cary 14 spectrophotometer with OLIS 14 version 2.6.99 operating system. ^{1}H and ^{31}P NMR spectra were collected using a Bruker ACP-300 spectrometer. IR spectra were recorded on Perkin-Elmer FT-IR 1760X spectrometer in KBr pellets. For dynamic NMR, standard relations such as: $k_{eq} = \pi\Delta\nu/2$ and $\Delta G^{\ddagger} = RT_c[22.96 + \ln(T_c/\Delta\nu)]$ (where T_c is the coalescence temperature, $\Delta\nu$ is the line width at half-height in Hz, and other terms are of usual significance) were used for estimating the rate of exchange and the energy barrier, respectively.[17]

Synthesis. Tp*MoO_2Cl was prepared as described elsewhere.[12] NMR (^{1}H, δ, ppm) in $CDCl_3$: 5.87 (s, 2H, Pz−H), 5.31 (s, 1H, Pz−H), 2.69 (s, 6H, CH_3), 2.65 (s, 3H, CH_3), 2.39 (s, 6H, CH_3), 2.37 (s, 3H, CH_3). IR (KBr, cm^{-1}): 3128 (w, Pz−H), 2963 (m, CH_3), 2929 (m, CH_3), 2547 (m, B−H), 988 (m, Mo=O), 930 (s, Mo=O), 900 (vs).

General Procedure for Synthesizing Tp*MoOCl(OPR_3). In a typical experiment, 100 mg (2.16×10^{-4} mol) of Tp*MoO_2Cl was suspended in 20 mL of benzene at room temperature. To this suspension, a 2-fold excess of the desired phosphine was added. The reaction mixture was then stirred for 10−30 min (∼10 min for PEt_3 and 30 min for PMe_3 or $PPhMe_2$) and filtered to remove any unreacted Tp*MoO_2Cl. The volume of filtrate was reduced to 2 mL, and the desired complex was precipitated by adding 5 mL of hexane into the filtrate. The solvent mixture was refrigerated for 0.5−2 h; the target Tp*MoOCl(OPR_3) complex was filtered, washed with hexane, and dried in a vacuum.

Tp*MoOCl($OPMe_3$). Yield: 64 mg (55%) recovered Tp*MoO_2Cl: 28 mg (28%). NMR (^{1}H, σ, ppm) in C_6D_6: 5.82 (s, 1H, Pz−H), 5.74 (s, 1H, Pz−H), 5.53 (s, 1H, Pz−H), 3.03 (s, 3H, Me), 2.81 (s, 3H, Me), 2.66 (s, 3H, Me), 2.31 (s, 3H, Me), 2.26 (s,

(10) Kail, B. W.; Perez, L. M.; Zaric, S. D.; Millar, A. J.; Young, C. G.; Hall, M. B.; Basu, P. submitted for publication.
(11) (a) Seymore, S. B.; Brown, S. N. *Inorg. Chem.* **2000**, *39*, 325−332. (b) Sung, K.-M.; Holm, R. H. *J. Am. Chem. Soc.* **2002**, *124*, 4312−4320.
(12) (a) Xiao, Z.; Bruck, M. A.; Enemark, J. H.; Young, C. G.; Wedd, A. G. *Inorg. Chem.* **1996**, *35*, 7508−7515. (b) Roberts, S. A.; Young, C. G.; Kipke, C. A.; Cleland, W. E., Jr.; Yamanouchi, K.; Carducci, M. D.; Enemark, J. H. *Inorg. Chem.* **1990**, *29*, 3650−3656.
(13) Millar, A. J.;. Doonan, C. J.; Smith, P. D.; Nemykin, V. N.; Basu, P.; Young, C. G. *Chem. Eur. J.* **2005**, *11*, 3255−3267.
(14) Smith, P. D.; Millar, A. J.; Young, C. G.; Ghosh, A.; Basu, P. *J. Am. Chem. Soc.* **2000**, *122*, 9298−9299.
(15) Nemykin, V. N.; Laskin, J.; Basu, P. *J. Am. Chem. Soc.* **2004**, *126*, 8604−8605.
(16) Basu, P.; Nemykin, V. N.; Sengar, R. *Inorg. Chem.* **2003**, *42*, 7489−7501.
(17) Sandstroem, J. In *Dynamic NMR Spectroscopy*; Academic Press: London, 1982.

3H, Me), 2.13 (s, 3H, Me), 1.35 (d, 9H, PMe_3, $^3J_{PH}$ = 13 Hz); ^{31}P (C_6D_6): 65 ppm. IR (KBr, cm^{-1}): 3126 (w, Pz−H), 2956 (m, Me), 2921 (m, Me), 2854 (m, P−Me), 2521 (m, B−H), 1108 (s) (P═O), 955 (s, Mo═O). UV−vis in acetonitrile, λ, cm^{-1} (ϵ, M^{-1} cm^{-1}): 12 200 (58), 23 700 (111), 30 400 (1060); in toluene, λ, cm^{-1}: 12 200, 23 600, 29 900. ESI MS (*m*/*z*, acetonitrile): 538 (100%) $[M]^+$ calcd for $C_{24}H_{36}N_6O_2BMoPCl$.

Tp*MoOCl(OPEt$_3$). Yield: 42 mg (33%), recovered Tp*MoO_2Cl: 47 mg (47%). NMR (^1H, σ, ppm) in C_6D_6: 5.84 (s, 1H, Pz−H), 5.73 (s, 1H, Pz−H), 5.54 (s, 1H, Pz−H), 3.02 (s, 3H, CH_3), 2.89 (s, 3H, CH_3), 2.71 (s, 3H, CH_3), 2.31 (s, 3H, CH_3), 2.26 (s, 3H, CH_3), 2.11 (s, 3H, CH_3), 2.08 (dq, 6H, P−**CH**$_2$−CH_3, $^3J_{HH}$ = 7.5 Hz), 1.72 (dq, 6H, P−**CH**$_2$−CH_3, $^3J_{HH}$ = 7.5 Hz), 0.88 (dt, 9H, P−CH_2−**CH**$_3$, $^3J_{HH}$ = 7.5 Hz); ^{31}P: 78 ppm. IR (KBr, cm^{-1}): 3079 (w, Pz−H), 2973 (m, CH_3), 2975 (m, CH_3), 2884 (m, CH_2), 2850 (m, CH_2), 2524 (m, B−H), 1090 (vs) (P═O), 950 (vs, Mo═O). UV−vis in acetonitrile, λ, cm^{-1} (ϵ, M^{-1} cm^{-1}): 12 100 (54), 23 400 (114), 30 100 (1129). ESI MS (*m*/*z*, acetonitrile): 580 (100%) $[M]^+$ calcd for $C_{27}H_{42}N_6O_2BMoPCl$.

Tp*MoOCl(OPPhMe$_2$). Yield: 56 mg (43%), recovered Tp*MoO_2Cl: 41 mg (41%). NMR (^1H, σ, ppm) in C_6D_6: 7.38−7.30 (m, 2H, *m*-Ph−H) 7.09−7.04 (m, 1H, *p*-Ph−H), 6.97−6.95 (m, 2H, *o*-Ph−H), 5.80 (s, 1H, Pz−H), 5.75 (s, 1H, Pz−H), 5.55 (s, 1H, Pz−H), 3.08 (s, 3H, Tp−CH_3), 2.69 (s, 3H, Tp−CH_3), 2.67 (s, 3H, Tp−CH_3), 2.32 (s, 3H, Tp−CH_3), 2.26 (s, 3H, Tp−CH_3), 2.14 (s, 3H, Tp−CH_3), 2.01 (d, P−CH_3, $^3J_{PH}$ = 15 Hz), 1.88 (d, P−CH_3, $^3J_{PH}$ = 15 Hz,); ^{31}P: 70 ppm. IR (KBr, cm^{-1}): 3057 (w, Pz−H), 2977 (m, C−H, Me), 2913 (m, C−H, Me), 2536 (m, B−H), 1087 (vs) (P═O), 945 (vs, Mo═O). UV−vis in acetonitrile, λ, cm^{-1} (ϵ, M^{-1} cm^{-1}): 12 100 (41), 22 700 (92), 28 300 (762). ESI MS (acetonitrile): 600 (100%) $[M]^+$ calcd for $C_{27}H_{42}N_6O_2BMoPCl$.

General Procedure for Synthesizing Tp*MoOCl(solv). In a typical experiment, at room temperature, 100 mg (2.16×10^{-4} mol) of Tp*MoO_2Cl was suspended in 20 mL of acetonitrile or dmf, to which a 2-fold excess of PPh_3 was added. The reaction mixture was stirred for 40 min, and the unreacted Tp*MoO_2Cl complex was filtered off. The volume of the filtrate was reduced to 0.5 mL at a reduced pressure, and the desired complexes were precipitated by adding a benzene/hexane mixture (1:2 v/v, 15 mL) and keeping the resultant mixture in a refrigerator for 0.5−2 h. Crystalline Tp*MoOCl(solv) complexes were filtered, washed with hexane several times, and dried in a vacuum at room temperature.

Tp*MoOCl(CH_3CN). Yield: 61 mg (58%), recovered Tp*MoO_2Cl: 6 mg (6%). NMR (^1H, σ, ppm) in C_6D_6/toluene-d_8: 5.77 (s, 1H, Pz−H), 5.69 (s, 1H, Pz−H), 5.42 (s, 1H, Pz−H), 2.93 (s, 3H, CH_3), 2.84 (s, 3H, CH_3), 2.51 (s, 3H, CH_3), 2.24 (s, 3H, CH_3), 2.19 (s, 3H, CH_3), 2.07 (s, 3H, CH_3); CD_3CN: 6.07 (s, 1H, Pz−H), 6.03 (s, 1H, Pz−H), 5.60 (s, 1H, Pz−H), 3.01 (s, 3H, coordinated AN), 2.68 (s, 3H, CH_3), 2.50 (s, 3H, CH_3), 2.48 (s, 3H, CH_3), 2.40 (s, 3H, CH_3), 2.29 (s, 3H, CH_3), 2.21 (s, 3H, CH_3). IR (KBr, cm^{-1}): 3124 (w, Pz−H), 2983 (m, C−H, Me), 2924 (m, C−H, Me), 2549 (m, B−H), 2250 (w, CN), 959 (vs, Mo═O). UV−vis in acetonitrile, λ, cm^{-1} 11 500sh (32), 13 830 (65), 26 810sh (213), 31 250sh (2167).

Tp*MoOCl(dmf). Yield: 42 mg (38%), recovered Tp*MoO_2Cl: 4 mg (4%). NMR (^1H, σ, ppm) in C_6D_6: 8.76 (s, 1H, O═C−H), 5.85 (s, 1H, Pz−H), 5.76 (s, 1H, Pz−H), 5.53 (s, 1H, Pz−H), 3.07 (s, 3H, N−CH_3), 2.87 (s, 3H, N−CH_3), 2.49 (s, 3H, CH_3), 2.32 (s, 3H, CH_3), 2.27 (s, 3H, CH_3), 2.21 (s, 3H, CH_3), 2.15 (s, 3H, CH_3), 1.76 (s, 3H, CH_3); in dmf-d_7: 8.75 (s, exchangeable with Dmf-d_7, O═C−H), 6.07 (s, 1H, Pz−H), 6.03 (s, 1H, Pz−H), 5.61 (s, 1H, Pz−H), 3.40 (s, exchangeable with dmf-d_7, N−CH_3), 3.20 (s, exchangeable with dmf-d_7, N−CH_3), 2.54 (s, 3H, CH_3), 2.51 (s, 6H, CH_3), 2.45 (s, 3H, CH_3), 2.26 (s, 3H, CH_3), 2.13 (s, 3H, CH_3). IR (KBr, cm^{-1}): 3120 (w, Pz−H), 3060 (w, Pz−H), 2957 (m, CH_3), 2925 (m, CH_3), 2544 (m, B−H), 1645 (vs, C═O), 958 (s) (Mo═O). UV−vis in acetonitrile, λ, cm^{-1}: 12 500 (40), 23 800sh (230), 28 100 (1018). ESI MS (acetonitrile): 519 (~70%, exchangeable with MeCN, overlapped with molybdenum-containing peak centered at 526) $[M]^+$.

Calculations. All computations were carried out using Gaussian 98W or 03W[18] and Hyperchem 6.03[19] software packages. The starting geometries were obtained by optimization with the PM3 Hamiltonian[20] implemented in the Hyperchem 6.03 program. These structures were used for the full optimization without any symmetry restrictions by density functional theory (DFT) implemented in the Gaussian 98W or 03W program. For DFT calculations, Becke's three-parameter hybrid exchange functional[21] and Lee−Yang−Parr nonlocal correlation functional[22] (B3LYP) were used. An effective core potential containing the LANL2DZ[23] or 3-21G(d)[24] basis set was applied to all atoms. For electronic structure calculations of Tp*MoOCl($OPMe_3$) and Tp*MoOCl($OPPhMe_2$), the X-ray-determined geometries were used. The electronic structures for all compounds were calculated using the B3LYP EC functional coupled with a DZVP basis set on molybdenum[25] and the 6-311G(d)[26] basis set for all other atoms. The charges on the atoms of interest were calculated using the Mulliken population analysis.[27] The percent atomic orbital contributions to molecular orbitals were calculated using the VMOdes program[28] from single-point energy calculations. The three-dimensional rotational barrier maps for the Tp*$Mo^{IV}OCl(OPR_3)$ complexes were calculated, starting from the DFT-optimized geometries, as the energy difference between the

(18) Frisch, M. J.; Trucks, G. W.; Schlegel, H. B.; Scuseria, G. E.; Robb, M. A.; Cheeseman, J. R.; Montgomery, J. A., Jr.; Vreven, T.; Kudin, K. N.; Burant, J. C.; Millam, J. M.; Iyengar, S. S.; Tomasi, J.; Barone, V.; Mennucci, B.; Cossi, M.; Scalmani, G.; Rega, N.; Petersson, G. A.; Nakatsuji, H.; Hada, M.; Ehara, M.; Toyota, K.; Fukuda, R.; Hasegawa, J.; Ishida, M.; Nakajima, T.; Honda, Y.; Kitao, O.; Nakai, H.; Klene, M.; Li, X.; Knox, J. E.; Hratchian, H. P.; Cross, J. B.; Bakken, V.; Adamo, C.; Jaramillo, J.; Gomperts, R.; Stratmann, R. E.; Yazyev, O.; Austin, A. J.; Cammi, R.; Pomelli, C.; Ochterski, J. W.; Ayala, P. Y.; Morokuma, K.; Voth, G. A.; Salvador, P.; Dannenberg, J. J.; Zakrzewski, V. G.; Dapprich, S.; Daniels, A. D.; Strain, M. C.; Farkas, O.; Malick, D. K.; Rabuck, A. D.; Raghavachari, K.; Foresman, J. B.; Ortiz, J. V.; Cui, Q.; Baboul, A. G.; Clifford, S.; Cioslowski, J.; Stefanov, B. B.; Liu, G.; Liashenko, A.; Piskorz, P.; Komaromi, I.; Martin, R. L.; Fox, D. J.; Keith, T.; Al-Laham, M. A.; Peng, C. Y.; Nanayakkara, A.; Challacombe, M.; Gill, P. M. W.; Johnson, B.; Chen, W.; Wong, M. W.; Gonzalez, C.; Pople, J. A. *Gaussian 03*, revision B.01; Gaussian, Inc.: Wallingford, CT, 2004.

(19) HyperChem Pro. 6.03, HyperCube, Inc.: Gainesville, FL, 2001.

(20) (a) *HyperChem Reference Manual*; HyperCube, Inc.: Gainesville, FL, 1996; p 637. (b) Stewart, J. I. P. *J. Comput.-Aided Mol. Des.* **1990**, *4*, 1−45.

(21) Becke, A. D. *Phys. Rev. A* **1988**, *38*, 3098−3100.

(22) Lee, C.; Yang, W.; Parr, R. G. *Phys. Rev. B* **1988**, *37*, 785−789.

(23) Hay, P. J.; Wadt, W. R. *J. Chem. Phys.* **1985**, *82*, 270−283, 284−298, 299−310.

(24) Pietro, W. J.; Francl, M. M.; Hehre, W. J.; Defrees, D. J.; Pople, J. A.; Binkley, J. S. *J. Am. Chem. Soc.* **1982**, *104*, 5039−5048. Dobbs, K. D.; Hehre, W. J. *J. Comput. Chem.* **1986**, *7*, 359−378. Dobbs, K. D.; Hehre, W. J. *J. Comput. Chem.* **1987**, *8*, 880−893.

(25) Basis sets were obtained from the Extensible Computational Chemistry Environment Basis Set Database, Version 4/22/01, developed and distributed by the Molecular Science Computing Facility, Environmental and Molecular Sciences Laboratory, Pacific Northwest Laboratory, P.O. Box 999, WA 99352, and funded by the U.S. Department of Energy. The Pacific Northwest Laboratory is a multiprogram laboratory operated by Battelle Memorial Institute for the U.S. Department of Energy under Contract No. DE-AC06-76RLO 1830.

(26) McLean, A. D.; Chandler, G. S. *J. Chem. Phys.* **1980**, *72*, 5639−5948. Krishnan, R.; Binkley, J. S.; Seeger, R.; Pople, J. A. *J. Chem. Phys.* **1980**, *72*, 650−654.

(27) Mulliken, R. S. *J. Chem. Phys.* **1955**, *23*, 1833−1840, 1841−1846, 2338−2342, 2343−2346.

Table 1. Crystallographic Data for Tp*MoOCl($OPMe_3$) and Tp*MoOCl($OPPhMe_2$)

	Tp*MoOCl($OPMe_3$)	Tp*MoOCl($OPPhMe_2$)
formula	$C_{21}H_{34}B_1Cl_1Mo_1N_6O_2P_1$	$C_{29}H_{39}B_1Cl_1Mo_1N_6O_2P_1$
cryst Class	monoclinic	monoclinic
space Group	$P2_{1/n}$	Cc
a, Å	13.099(8)	13.67(3)
b, Å	27.192(16)	16.59(2)
c, Å	8.263(6)	14.722(15)
β, (deg)	98.50(6)	91.88(13)
V, Å^3	2911(3)	3337(9)
Z	4	4
cryst size (mm)	0.06 × 0.10 × 0.80	0.1 × 0.15 × 0.17
reflns measured	13 389	3953
independent reflns	6700	3821
reflns used	2251 ($\sigma \geq 3.00$)	1673 ($\sigma \geq 2.00$)
R	0.071	0.076
R_w	0.161	0.160
$\Delta\rho_{max}$	1.24	0.78
GOF	0.935	0.984

most stable conformer and all other conformers obtained by changing the O−Mo−O−P (±40°) torsion angle or the Mo−O−P (±20°) angle with a 5° increment. To reduce the steric interactions between methyl groups of the coordinated OPR_3 and methyl groups of pyrazole rings, their atomic positions were optimized using a molecular mechanics approach with the MM^+ force field implemented in the HyperChem program. This step was followed by single-point calculations at the semiempirical PM3(tm) level using HyperChem software.

Crystallography. Green crystals of Tp*MoOCl($OPMe_3$) and Tp*MoOCl($OPPhMe_2$) complexes were grown from C_6H_6/hexane solutions of the compounds at −20 °C. Intensity data were collected at room temperature on a Rigaku AFC-7R diffractometer using Mo Kα radiation (0.71073 Å) and the ω:2θ scan technique. Corrections were made for polarization effects, absorption, and crystal absorption decay using standard TeXsan program.[29] The structures were solved using either Direct methods or the Patterson method and refined by full-matrix least-squares procedures on F^2 using the Crystals for Windows program.[30] For Tp*MoOCl($OPMe_3$), all nonhydrogen atoms were anisotropically refined with the exception of the disordered solvent benzene molecule. Initial refinement of a twinned crystal of Tp*MoOCl($OPPhMe_2$) yielded unsatisfactory displacement parameters and bond distances for the chlorine and the terminal oxo groups. Use of a disordered model, however, did not improve the structure and thus, the Mo═O and Mo−Cl distances should be used judiciously. In all cases, hydrogen atoms were included in the model at their idealized positions. Crystallographic data are summarized in Table 1, while bond distances and bond angles are presented in Table 4.

Results and Discussion

Synthesis and Characterization of Complexes. Reactions of Tp*MoO_2Cl with tertiary phosphines have been probed first by an ESI MS technique. Thus, when a solution of the oxidant Tp*MoO_2Cl reacted with a solution of phosphine (PMe_3, PEt_3, $PPhMe_2$, PPh_2Et, and PPh_3) and the reaction mixtures were probed by ESI MS, an intermediate of general formula Tp*MoOCl(OPR_3) could be detected. Interestingly, when trimesitylphosphine, was used as a substrate, no such intermediate complex could be detected by ESI MS. The apparent lack of reactivity of trimesitylphosphine under the experimental conditions is presumably due its large cone angle (212°)[31] that confers a small pocket (vide infra). The stability of the phosphoryl complexes in solution have been probed by ESI MS and ^{31}P NMR spectroscopy. Among the phosphoryl species tested, Tp*MoOCl($OPPh_3$) was found to be unstable under ESI MS conditions. This observation is consistent with attempted detection of this intermediate complex by ^{31}P NMR spectroscopy. While Tp*MoOCl($OPPh_3$) could be observed for a short period of time by ESI MS, no coordinated phosphine oxide could be detected by room-temperature ^{31}P NMR. In contrast, elimination of phosphine oxides from the green Tp*MoOCl(OPR_3) (OPR_3 = $OPMe_3$, $OPEt_3$, $OPhMe_2$) complexes has been found to be small in nonpolar organic solvents. Tp*MoOCl($OPMe_3$) has been found to be stable for more than an hour, while Tp*MoOCl($OPPh_2Et$) releases phosphine oxide within an hour (Supporting Information).

The solution studies discussed above provided insight to the stability of different phosphoryl species. Complexes Tp*MoOCl($OPMe_3$), Tp*MoOCl($OPEt_3$), and Tp*MoOCl($OPPhMe_2$) were isolated by reacting Tp*MoO_2Cl with 2 equiv of corresponding phosphines in noncoordinating solvents. However, similar complexes with bulkier phosphines PPh_2Et and PPh_3 could not be isolated. While the phosphoryl species of general formula Tp$^{i\mathrm{Pr}}$MoO(OAr)(OPR_3) could be prepared from the solvent coordinated species, Tp$^{i\mathrm{Pr}}$MoO(OAr)(solv),[13] the Tp*MoOCl(OPR_3) species could not be isolated from Tp*MoOCl(solv).

The infrared spectra of the Tp*MoOCl(OPR_3) complexes exhibit a B−H vibration at 2521−2536 cm^{-1} from the scorpionate ligand. The terminal molybdenum oxo group [ν(Mo═O)] resonance could be assigned at 945−955 cm^{-1}, and the coordinated phosphine-oxide [ν(P═O)] could be assigned at 1087−1108 cm^{-1}. The P═O vibration shifts ∼52−90 cm^{-1} lower in energy in the coordinated complexes as compared to the free phosphine oxide. Interestingly, the larger the phosphine cone angle (θ), the larger the shift: $OPMe_3$ (52 cm^{-1}) < $OPEt_3$ (76 cm^{-1}) < $OPPhMe_2$ (90 cm^{-1}). A similar shift of 76 cm^{-1} as has also been observed for Tp$^{i\mathrm{Pr}}$MoOCl($OPEt_3$),[13] reflecting close electronic structures for these compounds. This shift in the vibrational frequency agrees well with those reported earlier (10−100 cm^{-1}) for different phosphine oxide-coordinated complexes.[32] It is interesting to note that the ν(Mo═O) frequencies correlate linearly ($R^2 = 0.95$) with those of ν(P═O) frequencies in the Tp*MoOCl(OPR_3)—the lower the energy of the ν(P═O) vibration, the lower the energy of ν(Mo═O) vibration.

(28) Nemykin, V. N.; Basu, P. VMOdes: Virtual Molecular Orbital description program for Gaussian, GAMESS, and HyperChem, revision A 7.1, 2004.
(29) TeXsan 10.3b program; Rigaku, Inc. 1997.
(30) Betteridge, P. W.; Carruthers, J. R.; Copper, R. I.; Prout, K.; Watkin, D. J. *J. Appl. Crystallogr.* **2003**, *36*, 1487.
(31) Tolman, C. A. *Chem. Rev.* **1977**, *77*, 313−348.
(32) de Bolster, M. W. G. In *Topics in Phosphorus Chemistry*; Grayson, M., Griffith, E. J., Ed.; Wiley-Interscience: New York, 1983; Vol. 11, pp 69−296. Hooge, N.; Christen, P. J. *Rec. Trav. Chim. Pay-Bas* **1958**, *77*, 911−922. Goggin, P. L. In *Comprehensive Coordination Chemistry*; Wilkinson, G., Gillard, J. A., McCleverty, J. A., Eds.; Pergamon: Oxford, 1987; Vol. 2, pp 487−503. Cotton, F. A.; Barnes, R. D.; Bannister, E. *J. Chem. Soc.* **1960**, 2199−2203.

Table 2. ^{31}P Parameters for Tp*MoOCl(OPR$_3$) in CDCl$_3$

		δ, ppm (relative to 85% H_3PO_4)			
	Θ^a	PR_3	Tp*MoO(OPR$_3$)Cl	OPR_3	Δ^b
PMe_3	118	−62	65	38	127
PEt_3	132	−20	78	48	98
$PPhMe_2$	122	−45	59	33	104
PPh_2Et	140	−11	58	33	69
PPh_3	145	−6	−	26	−

[a] Reference 31. [b] Difference in chemical shifts between the coordinated phosphine oxide and noncoordinated phosphine.

The ^{1}H NMR spectra of Tp*MoOCl(OPR$_3$) clearly show effective C_1 symmetries in these molecules. In each case, the spectrum consists of three singlets (5.5−6.0 ppm) for the aromatic protons of the pyrazole rings, along with six singlets between 2.0 and 3.2 ppm from the methyl groups. In the case of Tp*MoOCl(OPPhMe$_2$), the diastereotopic methyl protons of OPPhMe$_2$ ligand are observed at 1.88 and 2.01 ppm with $^3J_{PH} \approx 15$ Hz. A similar situation has also been observed for Tp*MoOCl(OPEt$_3$) where the diastereotopic methylene protons resonate at 1.72 and 2.08 ppm. The methyl groups of OPEt$_3$ in this complex resonate as a doublet of triplets at 0.95 ppm. Finally, in the case of Tp*MoOCl(OPMe$_3$), the two diastereotopic doublets overlap with each other and are observed as a multiplet at 1.35 ppm. The nature of this multiplet has been further probed by variable-temperature ^{1}H NMR technique. As temperature is lowered, the coordinated OPMe$_3$ that appeared as a doublet at room temperature first broadens with a coalescent point at 210 K and then splits into two signals. This behavior reflects the rotation of the coordinated OPMe$_3$ ligand. From the variable-temperature NMR data, the rate of rotation at 210 K has been estimated to be 73 s^{-1} with an activation energy ($\Delta G^{\ddagger}$) of 10.35 kcal/mol.

The solution stability of the intermediate compounds was also probed by ^{31}P NMR spectroscopy (Table 2). At room temperature, benzene solutions of Tp*MoOCl(OPEt$_3$) release 30% of free OPEt$_3$ within an hour. In contrast, even after 5 h only ∼25% of free OPMe$_3$ could be detected from the benzene solution of Tp*MoOCl(OPMe$_3$). Considering the pK_b for both OPMe$_3$ and OPEt$_3$ is ∼16,[33] the observed difference in the phosphine-oxide dissociation is likely to be due to the differences in the steric properties of the phosphine-oxide ligands. The cone angle for PEt$_3$ (132°) is larger than that of PMe$_3$ (118°), which suggests the inherent difference in stability. It is interesting to note that the peak position of the coordinated phosphine-oxide is independent of the scorpionate and the equatorial ligands. For example, the ^{31}P resonance for coordinated OPEt$_3$ appeared at the same position in Tp*MoOCl(OPEt$_3$) and in Tp^{iPr}MoO(XR)(OPEt$_3$).[13]

The ESI MS of Tp*MoOCl(OPR$_3$) confirms the molecular formulation of the compounds in solution. In all cases, the molecular ion peak is only observable at a very low cone voltage and only with freshly prepared solutions. An increase in the cone voltage increases the collision energy[34] and leads to the dissociation of phosphine-oxide, suggesting that the Mo−O(P) bond is the weakest bond. This trend is in agreement with the gas-phase quantum mechanical calculations. Our recent SID MS experiment on Tp*MoOCl(OPMe$_3$) indicates that the bond dissociation energy for the Mo−O(P) bond is ∼29 kcal/mol,[15] while a value of 8.4 kcal/mol was obtained from a semiempirical calculation.[44] Clearly, the semiempirical calculation underestimates the bond dissociation energy.

The UV−visible spectra of Tp*MoOCl(OPR$_3$) were recorded in freshly prepared solutions in acetonitrile or toluene, and similar features were observed in both solvents. The band positions are listed in Table 3, while the spectra are displayed in Figure 1. In all cases, the spectra exhibit two low-intensity bands at ∼12 000 and 23 000 cm^{-1} and one intense band at ∼30 000 cm^{-1}. The first band has been tentatively assigned to $d_{xy} \rightarrow d_{xz}$ and $d_{xy} \rightarrow d_{yz}$ transitions on the basis of its intensity. From ligand-field theory, the d orbitals in oxo-molybdenum complexes are expected to follow the order $d_{xy} < d_{xz} \approx d_{yz} < d_{x^2-y^2} < d_{z^2}$, which agrees well with the density functional calculations. According to this description, the lowest-energy $d_{xy} \rightarrow d_{xz}$ transition should be very close in energy to the $d_{xy} \rightarrow d_{yz}$ transition and the d_{xy} orbital is doubly occupied in low-spin Tp*MoOCl(OPR$_3$). The position of this band can be changed by substituting the coordinated phosphine-oxide with acetonitrile, dmf, or pyridine. The energy of the transition can also be influenced by changing the energy of the d_π orbitals. The former is expected if the energy of the in-plane d_{xy} orbital is affected by different ligand fields of equatorial ligands (OPR$_3$ or a solvent molecule). The band located ∼23 000 cm^{-1} may be assigned to the $d_{xy} \rightarrow d_{x^2-y^2}$ transition. The positions of the

(33) Greenwood, N. N.; Earnshaw, A. *Chemistry of the Elements*; Pergamon: Oxford, 1984.

(34) Nemykin, V. N.; Basu, P. *Inorg. Chim. Acta*, **2005**, *358*, 2876−2882.

(35) Carducci, M. D.; Brown, C.; Solomon, E. I.; Enemark, J. H. *J. Am. Chem. Soc.* **1994**, *116*, 11856−11868. McNaughton, R. L.; Helton, M. E.; Cosper, M. M.; Enemark, J. H.; Kirk, M. L. *Inorg. Chem.* **2004**, *43*, 1625−1637. McMaster, J.; Carducci, M. D.; Yang, Y. S.; Solomon, E. I.; Enemark, J. H. *Inorg. Chem.* **2001**, *40*, 687−702. McNaughton, R. L.; Tipton, A. A.; Rubie, N. D.; Conry, R. R.; Kirk, M. L. *Inorg. Chem.* **2000**, *39*, 5697−5706.

(36) Bendix, J.; Birkedal, H.; Bogevig, A. *Inorg. Chem.* **1997**, *36*, 2702−2703.

(37) Lever, A. B. P. *Inorganic Electronic Spectroscopy*, 2nd ed.; Elsevier Science Publishing: New York, 1986; p 864.

(38) Harden, N. C.; Humphrey, E. R.; Jeffrey, J. C.; Lee, S.-M.; Marcaccio, M.; McCleverty, J. A.; Rees, L. H.; Ward, M. D. *J. Chem. Soc., Dalton Trans.* **1999**, 2417−2426. Ung, V. A.; Couchman, S. M.; Jeffery, J. C.; McCleverty, J. A.; Ward, M. D. *Inorg. Chem.* **1999**, *38*, 365−369. Faller, J. W.; Ma, Y. *J. Organomet. Chem.* **1988**, *340*, 59−69. Bakar, M. A.; Hills, A.; Hughes, D. L.; Leigh, G. J. *J. Chem. Soc., Dalton Trans.* **1989**, 1417−1423. Rietzel, M.; Roesky, H. W.; Katti, K. V.; Schmidt, H.-G.; Herbst-Irmer, R.; Noltemeyer, M.; Scheldrick, G. M.; Symons, M. C. R.; Abu-Raqabah, A. J. *Chem. Soc. Dalton Trans.* **1990**, 2387−2392.

(39) Parkin, G. *Chem. Rev*. **1993**, *93*, 887−911. Desrochers, P. J.; Nebesny, K. W.; LaBarre, M. J.; Lincoln, S. E.; Loehr, T. M.; Enemark, J. H. *J. Am. Chem. Soc.* **1991**, *113*, 9193−9200. Mayer, J. M. *Chemtracts: Inorg. Chem.* **1991**, *3*, 115−117. Song, J.; Hall, M. B. *Inorg. Chem.* **1991**, *30*, 4433−4437.

(40) Cotton, F. A.; Kibala, P. A.; Miertschin, C. S. *Inorg. Chem.* **1991**, *30*, 548−553.

(41) Greenwood, N. N.; Earnshaw, A. In *Chemistry of the Elements*; Pergamon: Oxford, 1984.

(42) Basu, P. *Chemtracts: Inorg. Chem.* **2004**, *17*, 12−23. Nemykin, V. N.; Basu, P. *Inorg. Chem.* **2003**, *42*, 4046−4056.

(43) Carrano, C. J.; Chohan, B. S.; Hammes, B. S.; Kail, B. W.; Nemykin, V. N.; Basu, P. *Inorg. Chem.* **2003**, *42*, 5999−6007.

(44) Nemykin, V. N.; Basu, P. *Dalton Trans.* **2004**, 1928−1933.

Table 3. UV−Vis Spectra of Tp*MoOCl(OPR$_3$) and Tp*MoOCl(solv)

complex	solvent	λ, cm^{-1} (ϵ, M^{-1} cm^{-1})[a]
Tp*MoOCl(OPMe$_3$)	CH_3CN	12 200 (58), 23 700 (111), 30 400 (1060)
	toluene	12 200, 23 600, 29 900
Tp*MoOCl(OPEt$_3$)	CH_3CN	12 100 (54), 23 400 (114), 30 100 (1129)
Tp*MoOCl(OPPhMe$_2$)	CH_3CN	12 100 (41), 22 700 (92), 28 300 (762)
Tp*MoOCl($NCCH_3$)	CH_3CN	11 500sh (32), 13 830 (65), 26 810sh (213), 31 250sh (2167)
Tp*MoOCl(dmf)	CH_3CN	12 500 (40), 23 800sh, 28 100 (1018)

[a] sh = shoulder.

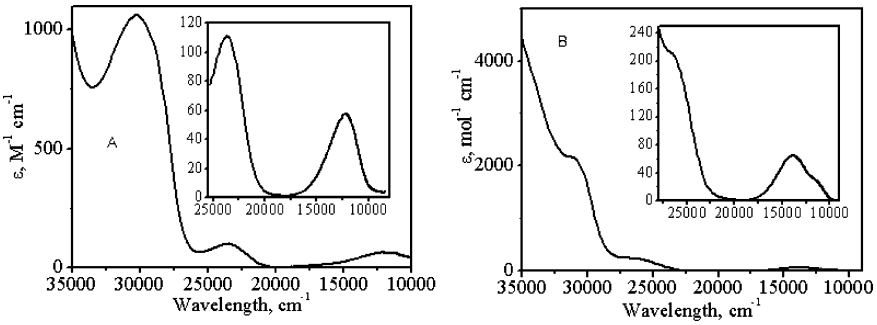

Figure 1. Room-temperature electronic spectra of Tp*MoOCl(OPMe$_3$) (A) and Tp*MoOCl(CH_3CN) (B) in acetonitrile.

first and second bands are similar to those observed for the low-spin monooxo molybdenum(V) and (IV) complexes where typically the first d−d transition ($d_{xy} \rightarrow d_{xz,yz}$) is observed between 11 000 and 15 000 cm^{-1}, while the second $d_{xy} \rightarrow d_{x^2-y^2}$ transition is usually located between 21 000 and 25 000 cm^{-1}.[35−37] The third band located at ∼30 000 cm^{-1} is probably due to ligand-to-metal charge-transfer transitions involving in-plane and out-of-plane orbitals of the chlorine ligand and the high-energy occupied π orbitals of the scorpionate ligand.

The UV−vis spectra of Tp*MoOCl(dmf) were recorded in fresh acetonitrile solutions at 4 °C in order to reduce any unwanted side reaction or solvent exchange process. The electronic spectrum of Tp*MoOCl(dmf) is close to those observed for Tp*MoOCl(OPR$_3$) and consists of two low-intensity bands at ca. 12 000 and 24 000 cm^{-1} and one intense band at ca. 28 000 cm^{-1}. By analogy with Tp*MoOCl(OPR$_3$), the first band has been assigned as $d_{xy} \rightarrow d_{xz}$ and $d_{xy} \rightarrow d_{yz}$ transitions, while the band located at ca. 24 000 cm^{-1} has been attributed to the next d−d transition ($d_{xy} \rightarrow d_{x^2-y^2}$), and the third band located at ca. 28 000 cm^{-1} probably consists of several ligand-to-metal charge-transfer transitions involving the in-plane and out-of-plane orbitals of chlorine and occupied orbitals of Tp*. In Tp*MoOCl(MeCN), the low-energy d−d transition has a prominent shoulder at the low-energy region (11 500 cm^{-1}), while the maximum is located at 13 800 cm^{-1}, suggesting a nondegenerate d_π orbital set. The second d−d transition ($d_{xy} \rightarrow d_{x^2-y^2}$) is tentatively assigned at 26 800 cm^{-1}, which is shifted to higher in energy as compared to that in Tp*MoOCl(dmf) or Tp*MoOCl(OPR$_3$) (22700−23800 cm^{-1}). This high-energy shift reflects a stronger σ-donor character (and thus destabilization of the $d_{x^2-y^2}$ orbital) of acetonitrile as compared to dmf or OPR$_3$. Indeed, ΔE (defined as the difference between energies of $d_{xy} \rightarrow d_{xz,yz}$ and $d_{xy} \rightarrow d_{x^2-y^2}$ transitions) is ∼2000 cm^{-1} larger for Tp*MoOCl($NCCH_3$), as expected for acetonitrile ligand versus dmf or OPR$_3$.[37]

Table 4. Selected Bond Distances and Angles for Tp*MoOCl(OPMe$_3$) and Tp*MoOCl(OPPhMe$_2$) Complexes

	Tp*MoOCl(OPMe$_3$)	Tp*MoOCl(OPPhMe$_2$)
Mo(1)−O(1), Å	1.723(10)	1.910(17)[a]
Mo(1)−Cl(1), Å	2.420(4)	2.340(7)[a]
Mo(1)−O(2), Å	2.158(9)	2.140(12)
O(2)−P(1), Å	1.503(9)	1.471(15)
Mo(1)−N(11), Å	2.385(10)	2.113(18)
Mo(1)−N(21), Å	2.155(11)	2.184(18)
Mo(1)−N(31), Å	2.125(11)	2.382(16)
O(1)−Mo(1)−O(2)°	96.6(4)	97.3(6)
O(1)−Mo(1)−Cl(1)°	105.1(4)	94.6(6)
O(1)−Mo(1)−N(31)°	93.9(5)	174.2(8)
O(1)−Mo(1)−N(11)°	169.5(5)	95.8(6)
O(1)−Mo(1)−N(21)°	93.0(5)	96.5(7)
Mo(1)−O(2)−P(1)°	134.1(5)	143.7(9)
O(1)−Mo(1)−O(2)−P(1)°	46.4	39.4

[a] Disordered.

The molecular structures of Tp*MoOCl(OPMe$_3$) and Tp*MoOCl(OPPhMe$_2$) were determined by single-crystal X-ray crystallography. The molecular structures for these complexes are displayed in Figure 2, while selected bond distances and angles are presented in Table 4. Both complexes exhibit distorted octahedral geometry with respect to the molybdenum center. In the case of Tp*MoOCl(OPMe$_3$), the Mo═O (1.723(10) Å) and Mo−Cl bond distances (2.420(4) Å) are consistent with molybdenum oxygen double bond distance and molybdenum-to-chlorine single bond distance. However, in Tp*MoOCl(OPPhMe$_2$), there is a positional disorder between the chlorine and oxygen atoms which preclude accurate determination of the bond distances. Such a disorder has been reported in a number of MoO$_x$Cl$_y$ fragments.[38,39] The Mo−O(P) and O−P distances are in the range of 2.140(12)−2.158(9) Å and 1.471(15)−1.503(9) Å, respectively. Similar Mo−O(P) distances were observed for other phosphoryl complexes of the pyrazolyl borate ligand.[13,15] The O−P distances are also close to those found in other phosphoryl complexes[40] and shorter than the O−P single bond distance as in P_4O_{10}.[41] The metric parameters are in good agreement with spectroscopic results, which suggest a

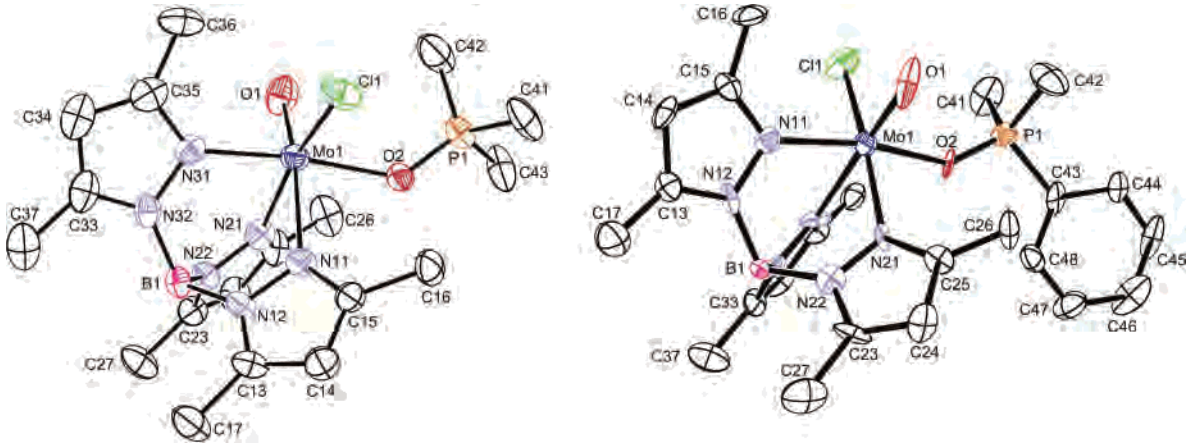

Figure 2. ORTEP diagram (at 30% probability) of Tp*MoOCl(OPMe$_3$) and Tp*MoOCl(OPMe$_2$Ph).

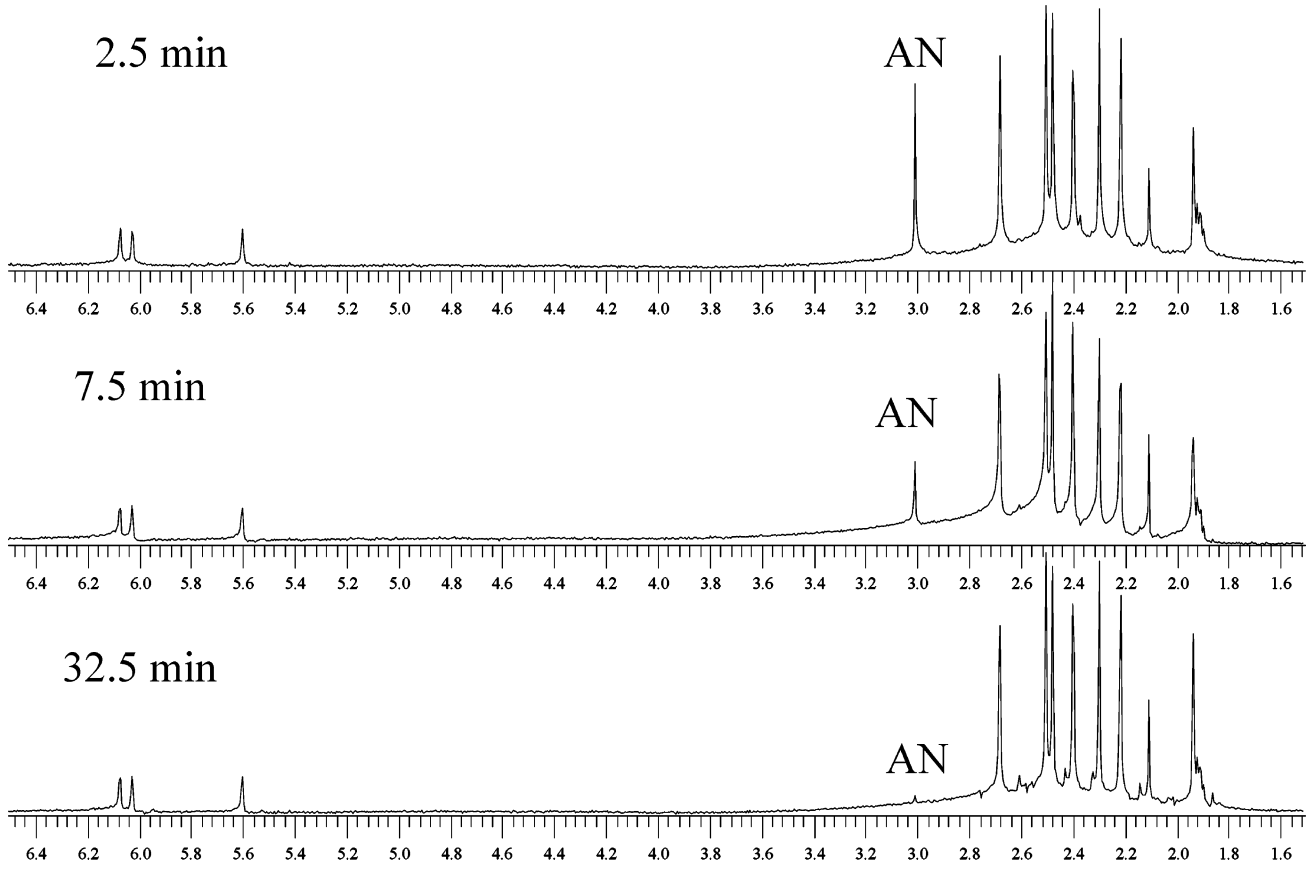

Figure 3. ^{1}H NMR spectra of Tp*MoOCl(CH$_3$CN) in CD$_3$CN as a function of time. The coordinated acetonitrile resonance has been labeled as AN.

reduced metal center. The observed Mo−O−P angles are 134.1° and 143.7°, while the O═Mo−O−P dihedral angles are 46.4° and 39.4° for Tp*MoOCl(OPMe$_3$) and Tp*MoOCl(OPPhMe$_2$), respectively. The long Mo−N (trans to the Mo═O group) distances in Tp*MoOCl(OPR$_3$) are consistent with the expected trans effect of the terminal Mo═O group. In comparison, the trans effect of the other groups can be arranged as O > Cl$^-$ > OPMe$_3$.

The infrared spectra of the Tp*MoOCl(solv) complexes exhibit B−H and C═N vibrations 2544−2549 and 1541−1543 cm^{-1}, respectively. The Mo═O vibrations appear at 958−959 cm^{-1}. Both the B−H and the Mo═O vibrations observed at similar positions to those in Tp*MoOCl(OPR$_3$) complexes and do not behave as a good diagnostic marker for these complexes. Interestingly, the C≡N vibration at 2253 cm^{-1} in Tp*MoOCl(MeCN) is very close those observed for free acetonitrile (2250 cm^{-1}), while shift of the carbonyl C═O vibration mode in Tp*MoOCl(dmf) is ∼25 cm^{-1} as compared to free dmf (1645 versus 1671 cm^{-1}) and serves as a good marker for the dmf coordination.

^{1}H NMR data of Tp*MoOCl(solv) are in a good agreement with their effective C_1 symmetry. In each case, the spectrum consists of three singlets at 5.5−6.0 ppm due to the aromatic protons of the scorpionate ligand. In addition, six singlets due to the methyl groups were observed between 1.5 and 3.0 ppm. In the case of Tp*MoOCl(MeCN), the methyl group

Table 5. Calculated Energies and Orbital Compositions of the Molybdenum Complexes

		orbital composition, %				
orbital	energy, eV	Mo (d)	$O_{terminal}$	Cl	OPR_3	L
		Tp*MoOCl($OPMe_3$)[a]				
138 − HOMO	−3.927	81.3 (d_{xy})	0.5	5.9	3.4	8.8
139 − LUMO	−1.008	68.1 (d_{xz})	13.8	0.6	6.0	11.5
140 − LUMO +1	−0.827	65.2 (d_{yz})	13.3	5.2	1.0	15.4
		Tp*MoOCl($OPMe_3$)[b]				
126 − HOMO	−4.530	84.3 (d_{xy})	0.3	5.0	3.1	7.3
127 − LUMO	−1.552	68.3 (d_{xz})	11.5	0.4	6.9	12.9
128 − LUMO +1	−1.441	68.3 (d_{yz})	11.6	4.0	1.4	14.6
		Tp*MoOCl($OPMe_3$)[c]				
126 −HOMO	−4.484	84.2 (d_{xy})	0.4	4.0	4.3	7.1
127 − LUMO	−1.490	65.6 (d_{xz})	11.0	0.7	9.4	13.3
128 − LUMO +1	−1.441	69.3 (d_{yz})	11.8	3.2	2.3	13.4
		Tp*MoOCl($OPPhMe_2$)				
154 − HOMO	−3.806	79.1 (d_{xy})	0.3	7.7	3.9	8.9
155 − LUMO	−1.076	21.4 (d_{xz})	4.6	0.1	69.7	4.1
156 − LUMO + 1	−0.906	66.9 (d_{yz})	12.9	5.1	2.7	12.4
157 − LUMO + 2	−0.880	50.4 (d_{xz})	9.8	0.4	28.9	10.5
		Tp*MoOCl(MeCN)[d]				
112 HOMO	−4.696	77.2 (d_{xy})	0.4	10.3	3.7	8.4
113 − LUMO	−1.845	60.0 (d_{xz})	15.8	0.7	14.4	9.2
114 − LUMO + 1	−1.377	68.1 (d_{yz})	14.6	5.4	0.2	11.7

[a] Geometry from the X-ray structure. [b] Optimized geometry with 3-21G* basis set. [c] Optimized geometry with LANL2DZ basis set. [d] Optimized geometry with 3-21G* basis set.

of the coordinated acetonitrile ligand appears at 3.01 ppm in nonpolar solvents which exchanges with deuterated acetonitrile. The coordinated acetonitrile methyl group disappears within ~30 min (Figure 3), resulting in an estimated half-life of 8.8 min (Supporting Information). In the case of Tp*MoOCl(dmf), the peaks of the coordinated dmf ligand appear at 8.76 (aldehyde proton), 3.01, and 2.81 ppm (methyl groups). The last two resonances are similar to those observed for Tp^{iPr}MoO(SBu)(dmf) (2.95 and 2.79 ppm, respectively).[13] Qualitatively, solvent exchange reaction is faster in Tp*MoOCl(dmf) than in Tp*MoOCl(MeCN). When Tp*MoOCl(dmf) is dissolved in dmf-d_7, only small residual peaks of coordinated dmf-h_7 was observed for approximately 5 min.

Electrospray ionization mass spectrometry of freshly prepared solutions of Tp*MoOCl(solv) confirms the molecular nature of these compounds. In all cases, the molecular peak is the only observable ion at a low cone voltage. Interestingly, the coordinated dmf in Tp*MoOCl(dmf) is exchanged with acetonitrile, as evidenced by ESI MS. The ESI MS spectrum of this compound in acetonitrile exhibits two intense peak clusters with mass-to-charge ratios of ~560 and 528, which can be attributed to Tp*MoOCl(dmf) and Tp*MoOCl(MeCN), respectively. This observation is in contrast to that for Tp^{iPr}MoO(SBu)(dmf) for which the only Tp^{iPr}MoO(SBu)(MeCN) peak has been observed in the ESI MS spectrum.[13]

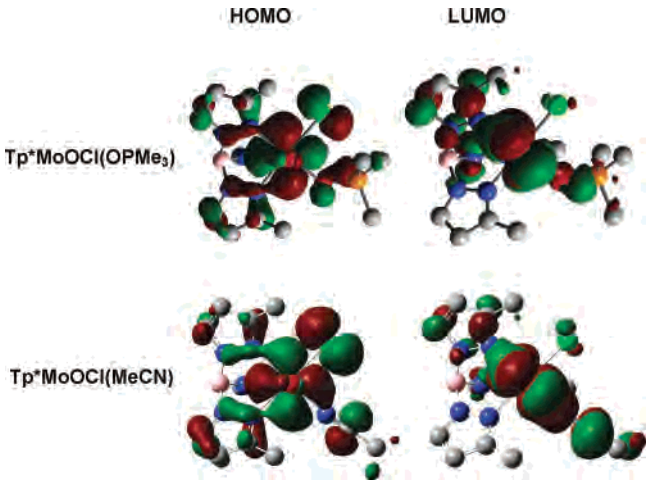

Figure 4. Graphical representation of the calculated HOMO and LUMO of Tp*MoOCl($OPMe_3$) and Tp*MoOCl(MeCN).

Electronic Structure and Rotational Barrier Calculations in Mo(IV) Complexes. The results of our DFT calculations on the Tp*MoOCl($OPMe_3$), Tp*MoOCl($OPPhMe_2$), and Tp*MoOCl(MeCN) are presented in the Tables 5 and 6. Because no X-ray crystal structure is available for the acetonitrile or dmf complex (Tp*MoOCl(solv)), we used the optimized geometry of Tp*MoOCl(MeCN) for electronic structure calculations. To understand whether the electronic structure calculated with the X-ray determined geometry differs significantly from that calculated with an optimized geometry, we have computed electronic structures with both geometries for Tp*MoOCl($OPMe_3$). First, the optimized structures using 3-21G* and LANL2DZ basis sets and are in reasonable agreement with the X-ray determined geometry (Table 6). Second, while in optimized structures, both the occupied and unoccupied orbitals are stabilized from those calculated for X-ray determined geometry; the relative energy differences between the orbitals are similar. Indeed, in all complexes, the order of the metal-centered orbitals is dictated by a single terminal oxo group.[42] The doubly occupied HOMO primarily consists of the Mo d_{xy} orbital (Figure 4). The LUMOs of both Tp*MoOCl($OPMe_3$) and Tp*MoOCl(MeCN) are nearly degenerate and consist of Mo d_{xz} and d_{yz} orbitals. For Tp*MoOCl($OPhMe_2$), however, the metal d_{xz} orbital is delocalized between the LUMO and the LUMO+2 as a result of phenyl ring π orbital and molybdenum d_{xz} orbital interaction. The same delocalization has also been observed in other Tp^{iPr}MoO(XR)(OPR_3) complexes.[13] For Tp*MoOCl($OPPhMe_2$), the difference in energy between the d_{xz} and the d_{yz} (LUMO to LUMO+2, respectively) can be gleaned from the UV−vis spectra. In this case, the first d−d band has been assigned to both $d_{xy} \rightarrow d_{xz}$ and $d_{xy} \rightarrow d_{yz}$ transitions, suggesting the energy difference between d_{xz} and d_{yz} orbitals is small. From DFT calculations,

Table 6. Calculated and Experimental Bond Distances and Angles for Tp*MoOCl($OPMe_3$)

	distance, Å					angle, deg	
geometry	Mo═O	Mo−O(P)	Mo−Cl	Mo−N	O−P	Mo−O−P	O−Mo−O−P
X-ray	1.72	2.16	2.42	2.13; 2.16; 2.39	1.50	134.1	46.4
3-21G*	1.71	2.19	2.51	2.15; 2.18; 2.38	1.54	128.2	55.0
LANL2DZ	1.72	2.16	2.56	2.16; 2.18; 2.39	1.66	127.5	58.9

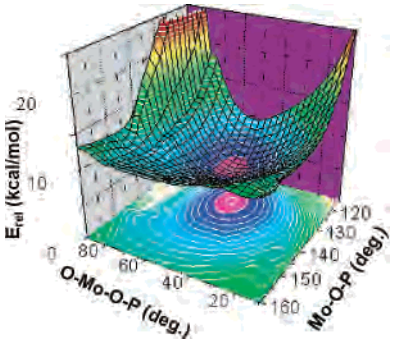

Figure 5. Three-dimensional energy surfaces for Tp*MoOCl(OPPhMe$_2$).

the energy difference between d_{xz} and d_{yz} orbitals in Tp*MoOCl(OPR$_3$) has a minimum value of 0.049 eV and a maximum value of 0.196 eV, which is consistent with experiments. On the other hand, the calculated energy difference between d_{xz} and d_{yz} orbitals in Tp*MoOCl(MeCN) is much larger (0.468 eV), which makes it visible as a shoulder in the first d−d band. Interestingly, the $d_{x^2-y^2}$ and d_{z^2} orbitals of Tp*MoOCl(OPR$_3$) are delocalized with the ligand-based orbitals, while such a delocalization is less prominent in Tp*MoOCl(MeCN).[13,43] In the phosphoryl compounds, the first occupied molecular orbital with significant contribution from the OPR$_3$ fragment is separated by ∼4 eV from the HOMO.

Our recent investigation[13] with the bulkier pyrazolyl borate ligand suggests that both the O−Mo−O−P torsion angle and Mo−O−P angle can influence the stability of the intermediate molecules through an '*energy-controlled pocket*'. At room temperature where thermal energy (*kT*) is ∼0.6 kcal/mol, rotational freedom is confined within a small area restricted by O−Mo−O−P and Mo−O−P angles, and with increasing steric bulk at the phosphine, this area decreases and eventually the coordination of bulky phosphine oxide ligands is not favored. In the present system, a small co-ligand (Cl) is used, and thus, the only difference among the compounds is in the phosphine oxide ligand. The calculated 3D energy surface for the Tp*MoOCl(OPR$_3$) complexes at the PM3(tm) semiempirical level (Figure 5) suggest that here also molecules are lying at the bottom of an energy-controlled pocket. As expected, the pocket is stabilized by the O−Mo−O−P and Mo−O−P angles and the *steric* restrictions imparted by the Tp* ligand. Accordingly, tris(mesityl)-phosphine does not react with Tp*MoO$_2$Cl under experimental conditions. In the absence of steric interaction, as would be case for planar ene-dithiolate ligands, no steric discrimination is expected. Our previous investigation[44] on such energy-controlled pockets suggest that Tp*MoOCl(OPMe$_3$) is more stable than [Tp*MoCl$_2$(OPMe$_3$)]$^+$, indicating [Mo^{VI}O]$^{4+}$ and [Mo^{VI}O$_2$]$^{2+}$ cores react differently. Thus, the steric interaction can influence the OAT reactivity.

Summary

OAT reactivity of Tp*MoO$_2$Cl has been examined with three different tertiary phosphines. The diamagnetic Mo(IV) phosphoryl compounds of general formula Tp*MoOCl(OPR$_3$) (OPR$_3$ = OPMe$_3$, OPEt$_3$, OPPhMe$_2$; Tp* = hydrotris(3,5-dimethylpyrazol-1-yl)borate) have been isolated and thoroughly characterized by spectroscopy and mass spectrometry, and two complexes have been crystallographically characterized (Tp*MoOCl(OPMe$_3$) and Tp*MoOCl(OPPhMe$_2$)). All data suggest that the metal center is in the reduced +4 state while the phosphorus is in the oxidized +5 state, and the phosphoryl complexes represent intermediate in the OAT reactions. The stability of the intermediate molecules depends on the steric properties of coordinated phosphine-oxides. In acetonitrile or dmf, the phosphoryl intermediate complexes generate solvated Tp*MoOCl(solv) complexes (solv = acetonitrile or dmf) via solvolysis reactions, and the coordinated solvents are exchangeable with bulk molecules.

In general, the behavior of the phosphoryl complexes with the Tp* ligand parallel those reported for the Tp^{i}Pr system. The structural features are very similar to each other, the synthetic strategies are similar, and the electronic structures of the molecules are similar. However, there are some distinct differences. For example, Tp*MoOCl(OPPh$_3$), where the phosphine is quite bulky, is yet to be isolated while Tp^{iPr}MoOCl(OPPh$_3$) has been structurally characterized. We attribute this difference due to the smaller pocket stabilized by the Tp* ligand. In addition, the phosphoryl species of general formula Tp^{iPr}MoO(OAr)(OPR$_3$) could be prepared from the solvent-coordinated species, Tp^{iPr}MoO(OAr)(solv),[13] however, the Tp*MoOCl(OPR$_3$) species could not be isolated from Tp*MoOCl(solv). The electronic spectra of Tp*MoOCl(OPR$_3$) exhibit distinct bands that changes by replacing the OPR$_3$ with MeCN or dmf. These bands are understood in terms of the electronic structure calculations.

Acknowledgment. Financial support from the National Institute of Health (GM 615502) is gratefully acknowledged (P.B.). We thank Prof. Charles Young for stimulating discussion.

Supporting Information Available: Crystallographic data in CIF format; tables of coordinates; and molecular orbital compositions. This material is available free of charge via the Internet at http://pubs.acs.org.

IC0508324